



HAL
open science

Quantification of coffinite (USiO₄) in roll-front uranium deposits using visible to near infrared (Vis-NIR) portable field spectroscopy

Benoît Hebert, Fabien Baron, Valentin Robin, Karl Lelievre, Nicolas Dacheux, Stephanie Szenknect, Adel Mesbah, Adrien Pouradier, Ruslan Jikibayev, Régis Roy, et al.

► To cite this version:

Benoît Hebert, Fabien Baron, Valentin Robin, Karl Lelievre, Nicolas Dacheux, et al.. Quantification of coffinite (USiO₄) in roll-front uranium deposits using visible to near infrared (Vis-NIR) portable field spectroscopy. *Journal of Geochemical Exploration*, 2019, 199, pp.53-59. 10.1016/j.gexplo.2019.01.003 . hal-02048827

HAL Id: hal-02048827

<https://hal.science/hal-02048827v1>

Submitted on 21 Oct 2021

HAL is a multi-disciplinary open access archive for the deposit and dissemination of scientific research documents, whether they are published or not. The documents may come from teaching and research institutions in France or abroad, or from public or private research centers.

L'archive ouverte pluridisciplinaire **HAL**, est destinée au dépôt et à la diffusion de documents scientifiques de niveau recherche, publiés ou non, émanant des établissements d'enseignement et de recherche français ou étrangers, des laboratoires publics ou privés.



Distributed under a Creative Commons Attribution - NonCommercial 4.0 International License

21 **Abstract:**

22 Coffinite ($USiO_4$) is a common uranium-bearing mineral of roll-front uranium deposits. This
23 mineral can be identified by the visible near infrared (Vis-NIR) portable field spectrometers
24 used in mining exploration. However, due to the low detection limits and associated errors,
25 the quantification of coffinite abundance in the mineralized sandstones or sandy sediments of
26 roll-front uranium deposits using Vis-NIR spectrometry requires a specific methodological
27 development.

28 In this study, the 1135 nm absorption band area is used to quantify the abundance of coffinite.
29 This absorption feature does not interfere with NIR absorption bands of any other minerals
30 present in natural sands or sandstones of uranium roll-front deposits. The correlation between
31 the 1135 nm band area and coffinite content was determined from a series of spectra
32 measured from prepared mineral mixtures. The samples were prepared with a range of
33 weighted amounts of arenitic sands and synthetic coffinite simulating the range of uranium
34 concentration encountered in roll-front uranium deposits.

35 The methodology presented in this study provides the quantification of the coffinite content
36 present in sands between 0.03 wt% to 1 wt% coffinite with a detection limit as low as 0.005
37 wt%. The integrated area of the 1135 nm band is positively correlated with the coffinite
38 content of the sand in this range, showing that the method is efficient to quantify coffinite
39 concentrations typical of roll-front uranium deposits. The regression equation defined in this
40 study was then used as a reference to predict the amount of natural coffinite in a set of
41 mineralized samples from the Tortkuduk uranium roll-front deposit (South Kazakhstan).

42

43 **Key Words: near infrared, portable field spectroscopy, coffinite, roll-front deposits, ore**
44 **exploration, mineral quantification**

45 **1. Introduction**

46 Field-based visible near infrared (Vis-NIR) reflectance spectroscopy has been routinely used
47 in mining exploration for over 30 years. It is a robust and low-cost technique that can be
48 applied in the field to identify minerals with absorption features between 350 and 2500 nm.
49 This technique can also be used to semi-quantify the abundance of the main minerals that are
50 encountered in the alteration halos surrounding the ore deposits. Several publications have
51 discussed the use of Vis-NIR spectroscopy to characterize ore (Ramanaidou et al., 2015; Dill
52 2016), to map the distribution of minerals associated with ore deposits through airborne or
53 space-borne hyperspectral sensors (Kruse et al., 2003) and to identify *in situ* gangue minerals
54 and associated alteration halos during mining exploration phases (Hunt and Ashley 1979;
55 Pontual et al., 1997; Herrmann et al., 2001; Hauff 2008). This technique has been recently
56 used for the exploration of volcanic-type uranium deposits (Xu et al., 2017) and
57 unconformity-type uranium deposits (Mathieu et al., 2017). In both cases, the identification of
58 alteration mineral zones has been used as proxies for uranium ore.

59 In addition, recent developments in the synthesis of uraniferous minerals (Clavier et al., 2014;
60 Mesbah et al., 2015) and in Vis-NIR spectroscopy (Baron et al., 2014) have showed that this
61 field technique is an efficient tool to identify minor amounts of uranium bearing minerals
62 within the coffinite-uraniothorite series in rocks surrounding uranium deposits. Moreover, the
63 determination of a spectral feature, which i) did not interfere with any other Vis-NIR bands of
64 most rock-forming minerals that occur with coffinite, and ii) remains unaffected by
65 compositional variation of the coffinite-thorite solid solution series (Baron et al., 2014), offers
66 new opportunities for a quantitative approach (Andrews et al., 2017).

67 The goal of this study is to use the 1135 nm absorption band area in order to: i) determine the
68 detection limit of coffinite in artificial sands made of mixtures of known proportions of quartz
69 and synthetic coffinite (which simulate the sandy formations hosting the uranium within the

70 roll-front); ii) determine a regression equation between the area of the 1135 nm absorption
71 band and the amount of synthetic coffinite mixed with quartz in sands mixtures; iii) use this
72 linear regression equation as a reference to quantify natural coffinite abundances in a set of
73 mineralized samples of the Tortkuduk uranium roll-front deposit (South Kazakhstan); and iv)
74 discuss the validity of the obtained quantification method using the mineralogical data of the
75 Tortkuduk uranium ore deposit.

76

77 **2. Geological context**

78 The Tortkuduk uranium roll-front deposit belongs to the Muyunkum mining district, one of
79 the major uranium deposits of the Shu Saryssu basin located in the South Kazakhstan
80 (Yazikov 2002; Dahlkamp 2013). Such uranium deposits are characterized by low-grade and
81 high tonnage reduced uranium mineralization hosted in roughly consolidated sand or
82 sandstones. Roll-front deposits are typically divided in two compartments named after the
83 redox condition prevailing in the sandy formations. Mineralization occurs at the redox
84 front whereas reduced compartments are located ahead of uranium mineralization. Oxidized
85 compartments are located behind and are typically depleted in uranium as the redox front
86 progresses toward reduced formations. Information on both the geology and the mineralogical
87 characteristics of the sandy formation hosting the roll-front uranium deposits of Tortkuduk are
88 reported in Ben Simon (2009), Munara (2012), Dahlkamp (2013), Mathieu et al. (2015) or
89 Robin et al. (2015a). According to these authors, Tortkuduk uranium mineralization is
90 dominated by very fine-grained coffinite minerals ($<1\mu\text{m}$) associated with sulphides (*e.g.*
91 pyrite, marcasite) and organic matter. The uranium mineralization is hosted in a thick middle
92 Eocene sand reservoir composed of sand channel accumulations in a coastal environment. The
93 sandy formations constitute the reservoir. They vary from a relatively simple arenitic to

94 arkosic mineralogical composition. Most of the uranium mineralization is hosted in fine-
95 grained to verycoarse-grained horizons of unconsolidated and highly permeable sands.

96

97 **3. Materials and methods**

98 **3.1. Natural sands from the Tortkuduk uranium roll-front deposit**

99 A total of 37 representative mineralized sand samples were collected from 14drill-cores which
100 intersected the sandy reservoir of the Tortkuduk deposit. The uranium content measured by
101 X-ray fluorescence (XRF) ranges from 200 to 6200 ppm.

102 The average mineralogy of the selected samples comprise 65 to 74 wt% quartz, 9.5 to 19wt%
103 alkali feldspars (*e.g.* microcline and minor albite), 5 wt% micas (*e.g.* muscovite, biotite), 5 to 9
104 wt% clay minerals (*e.g.* smectite and kaolinite) and less than 1 wt% accessory minerals which
105 include coffinite, pyrite, marcasite, anatase, tourmaline, ilmenite, zircon and calcite (Ben
106 Simon, 2009; Mathieu et al., 2015; Robin et al., 2015a). Minor gypsum and goethite also
107 occur in the oxidized compartments of the roll-front deposits (Munara 2012). According to
108 their grain size, these sands range from fine to medium-grained (*i.e.* 125 to 500 μm). The
109 mean chemical analysis of a representative column of mineralized sand from this reservoir has
110 been determined as follows: 87.07 wt% SiO_2 ; 5.97 wt% Al_2O_3 ; 1.28 wt% Fe_2O_3 ; 0.15 wt%
111 FeO ; 0.01 wt% MnO ; 0.26 wt% MgO ; 0.23 wt% CaO ; 0.56 wt% Na_2O ; 1.45 wt% K_2O ;
112 0.20 wt% TiO_2 ; 0.10 wt% P_2O_5 ; 0.18 wt% U; 0.23wt% S (Ben Simon 2009).

113 Coffinite is the most common type of uranium-bearing mineral in all the samples (Boulesteix
114 et al., 2015, Lach et al., 2015, Mathieu et al., 2015, Robin et al., 2015b). Uraninite
115 (pitchblende) and uranium-bearing alteration products of primary titaniferous minerals locally
116 complete the uranium mineralization (Mathieu et al., 2015). Coffinite was only identified in
117 the highly mineralized samples using X-ray diffraction (XRD) (Robin et al., 2015b), whereas

118 it was detected in each sample by scanning electron microscope observations coupled with
119 energy dispersive X-ray analyses (SEM/EDS) (Boulesteix et al., 2015, Lach et al., 2015,
120 Mathieu et al., 2015, Robin et al., 2015b).

121 **3.2. X-Rays Fluorescence measurements**

122 Chemical measurements were provided by the mining company, KATCO. The uranium
123 content of natural sands was measured using the Innov-X Omega hand held XRF analyzer
124 manufactured by Innov-X-Systems. The XRF readings were conducted in soil mode (*i.e.* a
125 two-beam mode employing an internal Compton Normalization calibration). Each analysis
126 lasted four minutes in total with 150 seconds using beam 1 conditions (heavy elements) and
127 90 seconds using beam 2 (light and transition elements).

128 **3.3. Mineralogical sand mixtures**

129 The sand mixtures consist of known amounts of quartz and coffinite and were designed to
130 simulate arenitic sands containing from 0.005 wt% up to 1 wt% of coffinite in addition to
131 quartz. To remain close to the field conditions, the sand mixtures were not ground at any stage
132 of the preparation.

133 The source of quartz for the preparation of the sand mixtures was Fontainebleau sand NE34, a
134 fine-grained natural arenitic sand (< 250 μm) containing more than 98wt% SiO_2 (Delfosse-
135 Ribay et al., 2004).

136 A purified synthetic coffinite with a chemical composition of the ideal, end-member coffinite
137 (USiO_4) was provided by the Institute for Chemical Separation of Marcoule (ICSM, France)
138 for the preparation of sand mixtures. It consists of purified and well characterized aggregates
139 of individual 80 nm-long crystals having the zircon structure type (tetragonal, $I4_1/amd$)
140 (Mesbah et al., 2015; Szenknect et al., 2016). In natural samples of the Tortkuduk uranium
141 roll-front deposit, coffinite also consists of very fine-grained particles (*i.e.* less than 1 μm).

142 Eight mixtures of coffinite sands were prepared for this study: seven of which had a total
 143 mass of 2.5g and a coffinite proportion of 1, 0.75, 0.5, 0.25, 0.1, 0.05, and 0.03 wt%
 144 respectively; and one with a total mass of 20g and a coffinite proportion of 0.005 wt%. The
 145 proportion of Fontainebleau sand used for the mixtures corresponds to the difference between
 146 the total mass and the coffinite proportion. The uranium content for each sand mixture was
 147 calculated based on the wt% of purified coffinite in each sample (Table 1).

148 The control of the sample homogeneity was decisive considering the very low amounts of
 149 coffinite added to the Fontainebleau sand for the preparation of the sand mixtures. The
 150 obtained reflectance data in the Vis-NIR domain, which were collected from a surface
 151 analysis, are representative of the whole sample only if the three-dimensional homogeneity of
 152 the sample is verified. The small crystal size of the synthetic coffinite facilitated its
 153 dissemination in the quartz grain material even with very low coffinite amounts. The
 154 mixtures were made by slowly stirring the vials (30 revolutions per minute) for 2 days prior to
 155 the analysis. Special attention was paid to the handling of the sand mixtures to prevent them
 156 from shaking, in order to limit the settling of coffinite grains toward the bottom of the
 157 vials due to the high density of coffinite crystals ($d=5.1 \text{ g/cm}^3$).

Sample	Fontainebleau sand (mg)	Coffinite (mg)	Coffinite (wt%)	Uranium (ppm)
SF-Co_0.0005	19999.00	1.00	0.005	36
SF-Co_0.03	2499.25	0.75	0.030	216
SF-Co_0.05	2498.75	1.25	0.050	360
SF-Co_0.10	2497.50	2.50	0.100	720
SF-Co_0.25	2493.75	6.25	0.250	1800
SF-Co_0.50	2487.50	12.50	0.500	3600
SF-Co_0.75	2481.25	18.75	0.750	5400
SF-Co_1.00	2475.00	25.00	1.000	7200

158

159 **Table 1:** Composition of sand mixtures and their calculated uranium content.

160

161 **3.4. Reflectance measurements**

162 The reflectance spectra were acquired using the ASD TerraSpec[®] 4 Standard-Res field
163 spectrometer and the Indico[®] Pro software. The spectrometer includes: i) a fixed diffraction
164 grating silicon (Si) array for the 350 to 1000 nm spectral region, and ii) two oscillating
165 diffraction grating monochromators with cooled single element indium gallium arsenide
166 (InGaAs) detectors for the 1000 to 2500 nm spectral region.

167 The spectral resolution of the detectors is 3 nm in the 350 - 1000 nm range and 10 nm in the
168 1000-2500 nm range. A contact probe that contains both the artificial lighting source (*e.g.*
169 halogen lamp) and the optic fiber was used to analyze the samples.

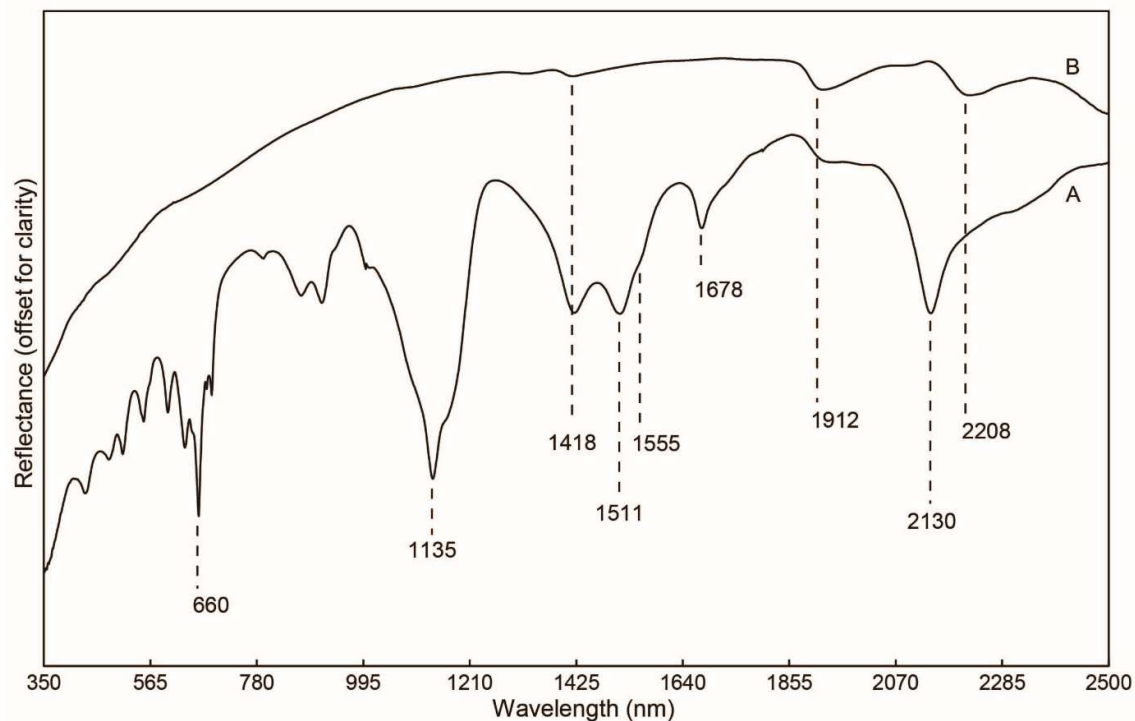
170 The spectrometer and the contact probe were switched on 30 minutes prior to the calibration and
171 the acquisitions to ensure the stabilization of both the detectors and the halogen lamp. Each
172 sample spectrum corresponds to the average of 50 stacked spectra acquired in about 7
173 seconds.

174 The samples were analyzed in two IR-transparent sample holders: i) sampling trays from the
175 ASD Muglight accessory and ii) small glass vials. Natural samples were also introduced into
176 the sample trays and measured without any preparation, as it is done in the field. The sand
177 mixtures were prepared and analyzed in the same vials. Reproducibility tests were performed
178 to ensure the homogeneity of the sand mixtures. The final Vis-NIR spectrum of each sample
179 was the average of six individual measurements, whereby the vial was turned over between
180 each reading to rearrange the sand mixtures. The number of six measurements was chosen as
181 the addition of more spectra do not impact significantly the final averaged spectrum (from
182 experiment). The high reproducibility of the Vis-NIR acquisitions validates the preparation
183 procedure of the prepared sands. The Spectral Geologist[™] (TSG[™]) software developed by the
184 CSIRO (CSIRO, 2017) was used in this study to visualize and analyze the spectral signature
185 of samples.

186 **4. Results and Discussion**

187 **4.1. Vis-NIR reflectance spectra of sand mixtures**

188 The Vis-NIR spectrum of the synthetic coffinite in sand mixtures is characterized by a series
189 of absorptions bands at 1135nm, 1418nm, 1511nm, 1678nm and 2130nm(Fig. 1A). The
190 absorption features occurring under 1800nm are attributed to the electronic transitions of the
191 U^{4+} in the octahedral position of minerals with a zircon-type crystal structure(*e.g.* zircon
192 ($ZrSiO_4$), thorite ($ThSiO_4$), coffinite ($USiO_4$)) and minerals of the thorite–coffinite solid
193 solution series reported as uranothorite(Mackey et al., 1975; Zhang et al., 2003, 2009; Baron
194 et al., 2014). To our knowledge, the multiple unusual sharp features observed between 350
195 and 700 nm are not described in the literature.



196

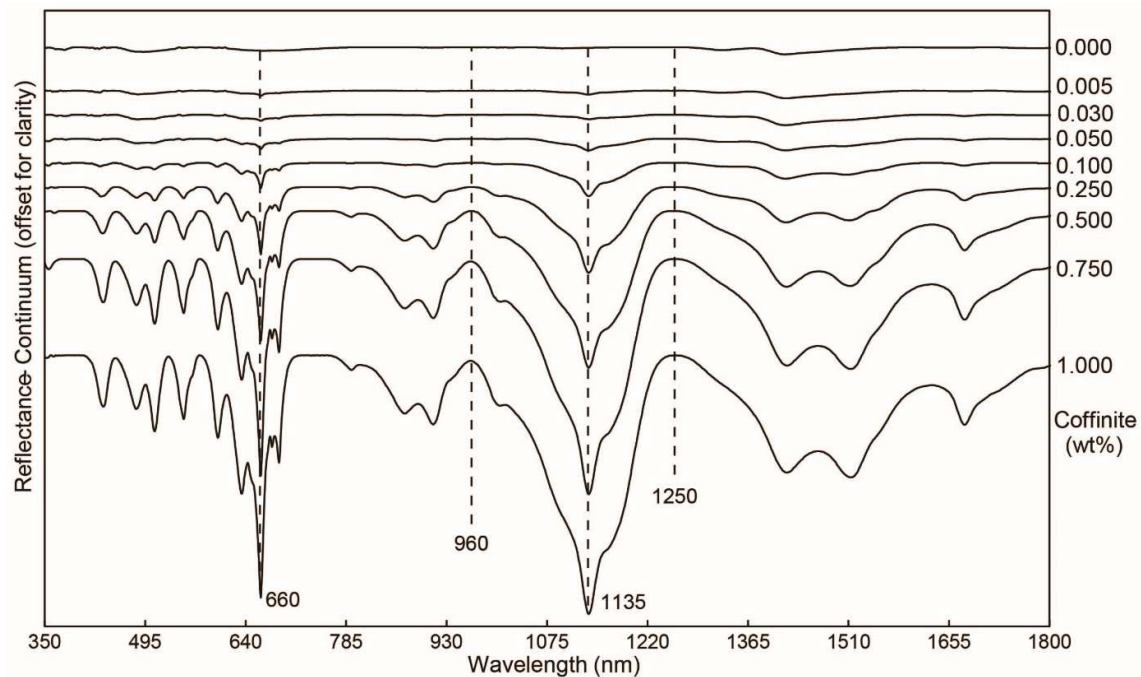
197 **Figure 1:** Vis-NIR reflectance spectra of both pure coffinite (A) and Fontainebleau sand (B) samples.
198 The vertical lines show the wavelength position of the major absorption features and are discussed in
199 the text.

200 Quartz is a spectrally transparent mineral in the Vis-NIR spectral range(Hunt and Salisbury
201 1970). However, spectra of pure Fontainebleau sand revealed the presence of weak absorption

202 bands at 1418 nm, 1912 nm and 2208 nm (Fig.1B). These features are due to very small
203 amounts of phyllosilicates (< 0.1 wt%) within the quartz grains (French and Worden 2013).
204 These bands are attributed to the combination modes of OH vibrations of water molecules at
205 1912 nm (Madejová et al., 2009) and to the first overtone and the combination modes of OH
206 vibrations of phyllosilicates near 1418 nm and 2208 nm, respectively (Post and Crawford
207 2014).

208 4.2. Quantification of coffinite in sand mixtures

209 The diagnostic absorption features of coffinite (*i.e.* 660 nm, 1135 nm, 1418 nm, 1511 nm,
210 1678 nm and 2130 nm absorption bands described in Fig. 1) are observed in the Vis-NIR
211 spectra of 8 sand mixtures in which the proportion of this mineral varies from 0.005 to 1 wt%
212 (Fig. 2).



213

214 **Figure 2:** Vis-NIR reflectance spectra of the sand mixtures. Continuum removal has been applied to
215 enhance differences in shape between spectra. The coffinite content is indicated in the side of each
216 sample spectrum. The vertical dash lines indicate the wavelength range used to integrate the area of
217 the 1135 nm band.

218

219 Coffinite can be detected in the reflectance spectrum of the sand mixtures from 0.005 wt%.

220 For low coffinite contents, two features can be observed in the spectra at 660 nm and 1135

221 nm. The continuum removed spectra enhance the identification of these two spectral features

222 in Figure 2, in particular for coffinite contents of 0.005 and 0.03 wt%.

223 Under TSGTM software two specific spectral parameters (or scalars) were created to quantify

224 the amount of coffinite from the 1135 nm and the 660 nm absorption bands.

225 Parameters were defined by isolating these bands from the overall shape of the spectrum using

226 the standard "continuum removal" (Clark and Roush 1984), also referred as "hull quotient" in

227 TSGTM. Relative absorption areas were integrated from: i) 960 nm to 1250 nm (*i.e.* the center

228 wavelength was set to 1105 nm and the search radius to 145 nm) and ii) from 575 nm to 750

229 nm, for the 1135 nm and the 660 nm features respectively.

230 Figure 3A and 3C shows positive linear correlations between the coffinite content and the

231 1135 nm and the 660 nm band area. The absorption feature at 1135 nm can be observed

232 unambiguously with coffinite contents of 0.05 wt% or higher in sand mixtures (Fig. 3B). A

233 positive linear correlation between the 660 nm and the 1135 nm band areas is logically

234 deduced as the coffinite content increase in the sand mixtures. Both bands could be used as a

235 spectral parameter to estimate the coffinite amount. However, for the same coffinite content,

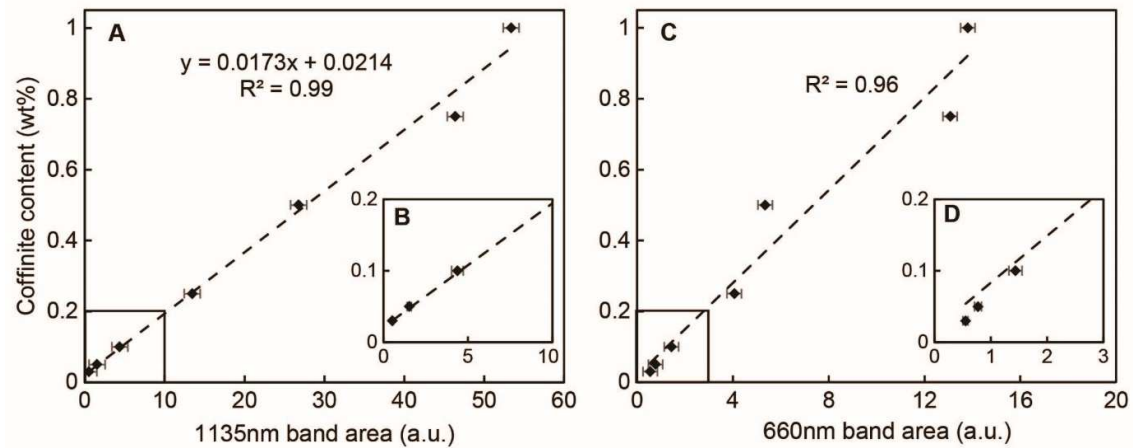
236 the 1135 nm band absorbs more than the 660 nm band. Natural sands usually contain a low

237 coffinite amount; therefore, it is imperative to use the band that shows the highest

238 absorption for coffinite content estimations. The average 1135 nm area (arbitrary unit, a.u.)

239 and the standard deviation calculated for 6 individual spectral readings per sample are

240 synthesized in Table 2.



241

242 **Figure 3:** Linear regressions between the integrated area of the 1135 nm band, the 660 nm band and the
 243 coffinite content of the sand mixtures.

244

245 The main factor of uncertainty for this method is due to the surface of the band, that slightly
 246 differs between the spectral readings conducted on the same sample. However, their standard
 247 deviation results showed an average area error of +/- 8% arbitrary units. Such low variations
 248 will not have a significant impact on its ability to estimate the coffinite content using Vis-NIR
 249 spectra.

250 Unlike the absorption bands near 1420 nm, the 1135 nm feature of coffinite does not interfere
 251 with any other band of a mineral occurring in natural sands (*e.g.* phyllosilicates features
 252 observed in Fig.4) and is a reliable marker of the coffinite content in the mineral mixtures.
 253 According to the Beer-Lambert law, the absorbance of a chemical bond is linearly related to
 254 its concentration in the structure of minerals composing a sample (Dahm and Dahm 2001).
 255 The use of diffuse reflectance spectrometers, such as the TerraSpec[®] 4 Standard-Res, may give
 256 rise to a non-linearity of the absorbance-concentration relation due to scattering effects
 257 (Gobrecht et al., 2015).

258 The 1135 nm integrated area values for the sand mixtures containing 0.005 and 0.03 wt%
 259 coffinite using the aforementioned method are significantly higher than that measured for the

260 pure Fontainebleau sand. However, the difference between the two values obtained for sand
 261 mixtures containing 0.005 and 0.03 wt% coffinite are not significantly different (Table 2).
 262 Such results suggest that coffinite can be detected but not quantified with the TerraSpec® 4
 263 Standard-Res spectrometer when its content in the sand mixture is lower than 0.03 wt%.

Sample	Average Area 1135 nm (a.u.)	Standard Deviation	Coffinite (wt%)	Uranium (ppm)
Pure sand	0.07	0.03	0.000	0
SF-Co_0.0005	0.47	0.05	0.005	36
SF-Co_0.03	0.52	0.07	0.030	216
SF-Co_0.05	1.53	0.20	0.050	360
SF-Co_0.10	4.38	0.08	0.100	720
SF-Co_0.25	13.45	1.13	0.250	1800
SF-Co_0.50	26.77	2.76	0.500	3600
SF-Co_0.75	46.38	1.19	0.750	5400
SF-Co_1.00	53.39	0.92	1.000	7200

264

265 **Table 2:** Integrated area of the 1135 nm band calculated with the TSG software and calculated
 266 uranium content from stoichiometry for sand mixtures.

267

268 For higher coffinite contents (*i.e.* from 0.03 to 1wt%), the area of the 1135 nm band (x)
 269 increases with the coffinite wt% following a linear regression equation (see Eq. 1) with a
 270 correlation coefficient equal to 0.99 (Fig.3A).

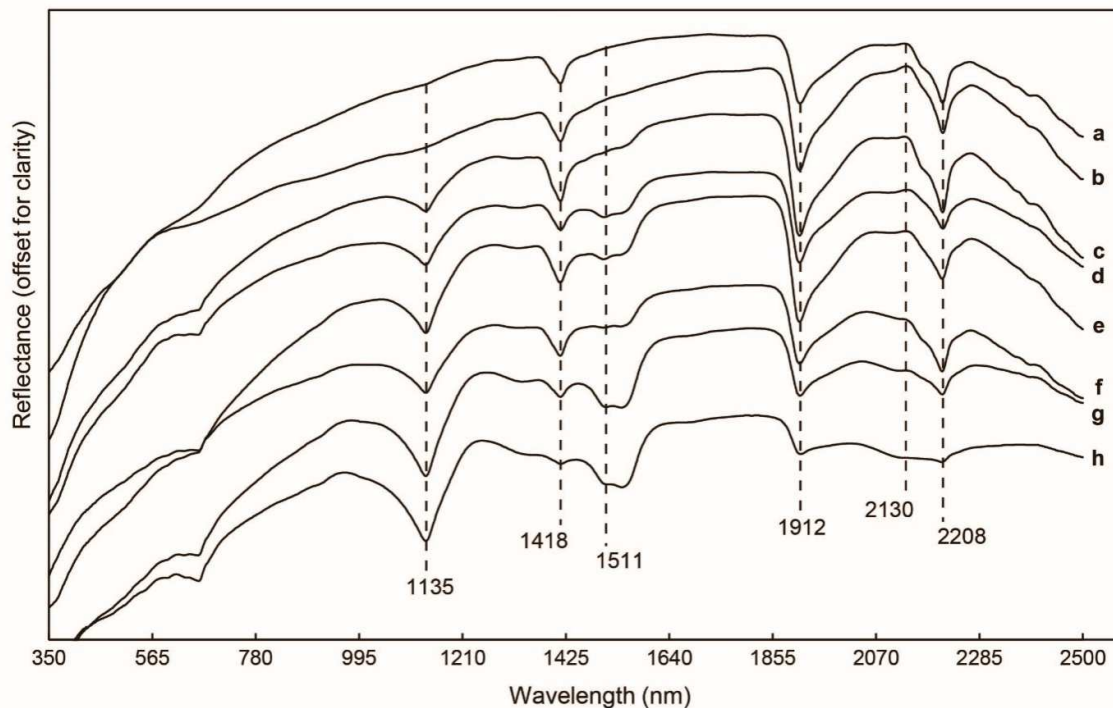
271
$$\text{Coffinite wt\%} = 0.0173x + 0.0214 \quad (\text{Eq. 1})$$

272 In summary, if such an empirical relationship is applied to an arenitic sand analogue, coffinite
 273 should be detected at concentrations as low as 0.005 wt%. Coffinite would be accurately
 274 quantified between 0.03 and 1 wt% using the integrated area of the absorption band at 1135
 275 nm.

276 **4.3. Quantification of coffinite in natural sands: application to the Tortkuduk uranium**
 277 **roll-front deposit**

278 The uranium content of the 37 mineralized samples from the Tortkuduk deposit, that were
279 measured by XRF, vary in the same range thanfor the sand mixturesthat were investigated in
280 the previous section (*i.e.* from 200 to 6200 ppm and from 0 to 7200 ppm, respectively). The
281 Vis-NIR spectra of eight mineralized sand samples are characterized by several coffinite and
282 phyllosilicate overlapping absorption features. The phyllosilicates consist of kaolinite,
283 muscovite and smectite (Robin et al., 2015a; Hebert et al., 2015) and their Vis-NIR spectra
284 exhibit strong absorption bands near 1418 nm, 1912 nm and 2208 nm and partially interfere
285 with the diagnostic bands of coffinite at 1418 nm, 1511 nm and 2130nm.
286 Note that substantial amounts of alkali feldspar (mostly microcline) can be encountered in
287 natural arkosic sands. Although these minerals can exhibit a weak absorptionfeature at 1210
288 nm due to the presence of Fe^{2+} in their structure (Anbalagan et al., 2009), this feature does not
289 overlap with the specific coffinite absorption band at 1135nm.

290



291

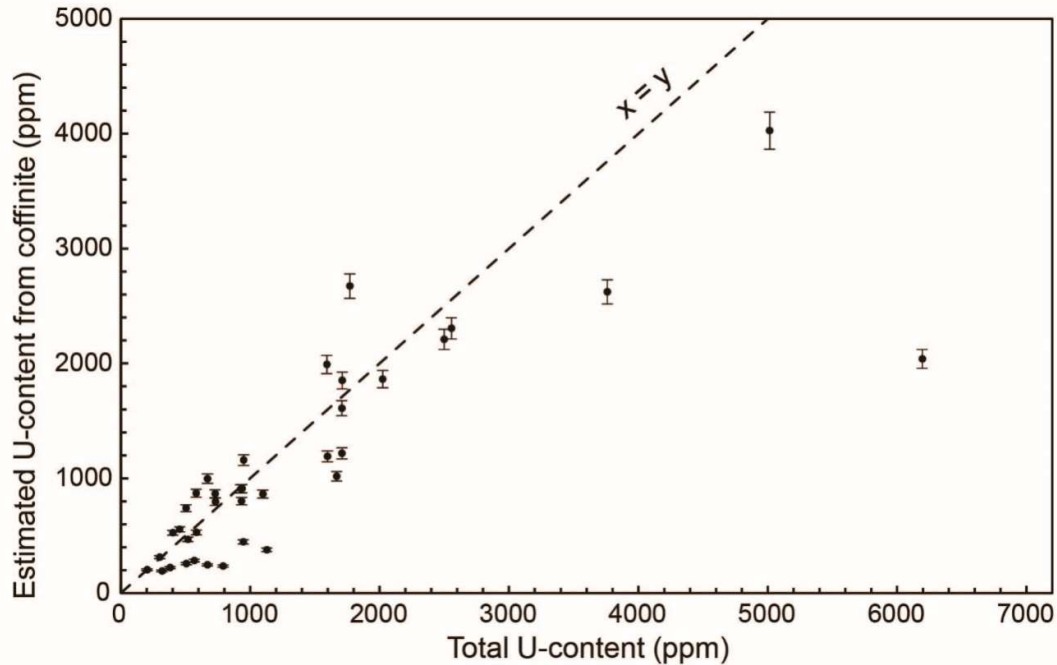
292 **Figure 4:** Vis-NIR reflectance spectra of representative mineralized samples from the Tortkuduk roll-
293 front uranium deposit. The vertical lines show the wavelength position of the major absorption
294 features and are discussed in the text.

295

296 The use of this methodology could be limited due to the partial overlap of the 1135 nm feature
297 of coffinite with broader absorption bands (centered between 350 and 1000 nm) related to
298 electronic transitions in ferric iron oxide and hydroxide minerals such as hematite, or goethite
299 (Ramanaidou et al., 2015). However, the local association of hematite or goethite with
300 coffinite is unexpected in natural sands due to their stability at very different redox conditions
301 (U^{4+} being oxidized into U^{6+} by Fe^{3+}). Coffinite crystallizes in reducing conditions and does
302 not co-exist with hematite or goethite when oxidizing conditions prevail. In the Tortkuduk
303 uranium deposit coffinite is restricted to the reduced section of the roll-front, whereas hematite
304 or goethite are identified in the absence of coffinite within the oxidized compartment, where
305 coffinite would dissolve and U^{6+} remobilized by the oxidizing solution (Szenknect et al.,
306 2016).

307 Such results demonstrate that the 1135 nm feature observed on natural mineralized sand
308 spectra appears to be the best candidate to quantify coffinite using Vis-NIR spectroscopy.

309 The coffinite content on Tortkuduk samples was determined empirically using Eq. 1
310 (established from the sand mixtures) and the 1135 nm band area calculated from the
311 mineralized sand spectra. Figure 5 shows the comparison between the uranium content
312 calculated from the resulting coffinite content and the bulk uranium content of natural sands
313 measured by XRF for each sample. Error bars represent the average standard deviation (4%)
314 of band area that was calculated from each of the 37 natural sample Vis-NIR spectra.



315

316 **Figure 5:** Comparison of the total uranium content measured by XRF to the estimated uranium
 317 content contained in coffinite only. The dashed line represents the theoretical regression line for which
 318 the total uranium content is incorporated as U^{4+} in coffinite ($USiO_4$).

319 Three main observations can be made based on the data presented Figure 5:

320 1) For a majority of samples (*i.e.* 24 over 37), the uranium content attributed to the coffinite
 321 using the quantitative method based on IR spectroscopy does not deviate significantly from
 322 the total uranium content measured by XRF in natural sands. This is particularly true for the
 323 mineralized samples in which the total uranium content does not exceed 2000 ppm.

324 2) According to the fact that the uncertainties in the quantification methods are not strictly
 325 controlled, there is no case in which the uranium content in coffinite exceeds significantly (*i.e.*
 326 overestimate by more than 1000 ppm of uranium) the total uranium content measured in the
 327 natural samples.

328 3) Conversely, several samples exhibited a content of uranium in coffinite significantly lower
 329 than the total uranium content in natural samples. This seems particularly the case for highest
 330 uranium grade samples (*i.e.* $5000 < \text{uranium} < 6200$ ppm).

331 The quantitative results obtained in this study from Vis-NIR spectroscopy are consistent with
332 the mineralogical characteristics of the mineralization encountered in the Tortkuduk uranium
333 roll-front deposit (Boulesteix et al., 2015, Mathieu et al., 2015). The good correlation that
334 exists between coffinite and the total uranium content of many natural sands agrees with the
335 identification of coffinite as being the most common uranium bearing mineral type within the
336 deposit (Mathieu et al., 2015).

337 For several samples and particularly for high-grade mineralization, the lowest uranium
338 content found in coffinite compared to the total uranium content of the sand could be explained
339 by the presence of additional uranium bearing minerals, such as primary titaniferous minerals
340 and/or uraninite (pitchblende) that have been identified at the core of the uranium mineralized
341 bodies (Mathieu et al., 2015). Unfortunately, uraninite (pitchblende) only show broad, low
342 intensity features in the 350 to 2500 nm range investigated by Vis-NIR portable field
343 spectrometers (Klunder et al., 2013).

344 Beside of the impact of additional uranium bearing mineral phases on the bulk uranium
345 content present in sands, it cannot be excluded that part of the coffinite, previously formed in
346 the mineralized zones, is now too amorphized to be fully identified by the Vis-NIR
347 spectroscopy. Self-irradiation related to uranium decay in radioactive minerals (emission of
348 alpha particles and their recoil effect) is known to damage the structure up to reach an
349 amorphous state (metamict state) with increasing time (Ewing 1994; Nasdala et al., 2005).
350 Infrared studies on the reverse process of reconstructing zircon from an initial amorphous
351 state showed an increase of intensity and complexity of the IR spectrum (Geisler et al., 2003).
352 Consequently, naturally occurring coffinite may have a reduced number of configurations that
353 can absorb in the Vis-NIR domain, lowering the level of available spectral information. The
354 potential impact of metamictisation on the quantification of coffinite is supported by the

355 $^{207}\text{Pb}/^{235}\text{U}$ ages of 2 to 20 My, which have been obtained for the mineralization of the
356 Tortkuduk uranium roll-front deposits (Mathieu et al., 2015).

357 The above considerations support the robustness of the method to quantify coffinite in roll-
358 front uranium deposits, which use the 1135 nm feature as a relevant spectral parameter.

359

360 **5. Conclusions**

361 The present study proposed a new methodology to quantify coffinite (USiO_4) abundance in
362 arenitic to arkosic sands or sandstones associated with roll-front uranium deposit using Vis-
363 NIR portable field spectroscopy.

364 Previous works identified a diagnostic feature in the Vis-NIR spectra of coffinite at 1135 nm
365 allowing a fast and convenient method to identify this mineral in complex mineralogical
366 mixtures of altered granite (Baron et al., 2014). This feature presents several advantages: i) it
367 does not interfere with any other Vis-NIR features of ubiquitous silicate minerals such as
368 phyllosilicates (clay minerals particularly), and ii) results from electronic transitions of the
369 U^{4+} cations in minerals with a zircon-type structure (Baron et al., 2014).

370

371 The coffinite content was determined using the 1135 nm feature measured from spectra
372 acquired on a series of sand mixtures of arenitic sand and purified synthetic coffinite. The high
373 correlation established between 1135 nm integrated area and the amount of coffinite in the
374 sand mixtures shows that this mineral can be accurately quantified for concentrations between
375 0.03 and 1.0 wt%. The detection limit is 0.005 wt% and it is consistent with the
376 concentrations encountered in the Tortkuduk uranium roll-front deposit. Note that such a
377 threshold is significantly lower than the one determined by Andrews et al. (2017) from Vis-

378 NIR spectra of complex mineral mixtures prepared to simulate a metasomatic albitite uranium
379 deposit of Australia.

380 The present methodology was then tested on natural samples from the Tortkuduk uranium
381 roll-front deposit. The results confirm that coffinite is the main uranium-bearing mineral in
382 most of the bulk samples uranium except in the higher-grade mineralization where uraninite
383 or uranium-bearing titaniferous minerals have been identified by previous mineralogical
384 investigations (Mathieu et al., 2015). This study demonstrates the efficiency and the high
385 sensitivity of the Vis-NIR spectroscopy for the detection and the quantification of coffinite in
386 uranium bearing sand or sandstone deposits. However, further works is required to: i) improve
387 the accuracy of the coffinite quantification at the Muyunkum mining district scale, and ii)
388 apply the proposed methodology to other worldwide sand or sandstone uranium deposits.

389 First, the uncertainty of the quantitative results obtained for the samples of Tortkuduk could
390 be improved by taking into account the grain size effect of other minerals (in particular quartz
391 and alkali feldspars) on the absorbency of coffinite. An additional linear regression equation
392 between at the 1135 nm integrated area and the coffinite concentrations in sandy sediments
393 for grain sizes ranging from fine to coarse is required.

394 As the detection limits varies with the mineral mixtures (Hauff 2008), the quantification of
395 coffinite in other worldwide sand or sandstone deposits requires the definition of specific
396 linear regression equations built from mineral mixtures representative as much as possible of
397 the mineralogy of the studied deposit.

398 Finally, even if the Vis-NIR spectroscopy is known as a suitable method to identify poorly
399 organized crystalline structures (Hauff 2008), experimental works would be necessary to
400 determine the effects of metamictisation on the 1135 nm band area of coffinite encountered in
401 natural uranium deposits.

402 **Acknowledgements**

403 The authors gratefully acknowledge R. Mathieu, M. Distinguin, Y. Deschamps, M. Brouand
404 and the geology team from KATCO Inc. for their previous work on the subject and for
405 providing advices, background, sample material, XRF analysis and logistic support as well as
406 the chemistry team from the ICSM laboratory for providing the synthetic coffinite. This work
407 has been financially supported by AREVA Mines and the NEEDS program.

408

409 **References**

- 410 Anbalagan, G., Sankari, G., Ponnusamy, S., kumar, R.T., Gunasekaran, S., 2009. Investigation of
411 silicate mineral sanidine by vibrational and NMR spectroscopic methods. *Spectrochim. Acta.*
412 *A. Mol. Biomol. Spectrosc.* 74, 404–409. doi:10.1016/j.saa.2009.06.034
- 413 Andrews, W.L., Tardio, J., Bhargava, S.K., Wilde, A., Otto, A., Pownceby, M.I., 2017. Development of a
414 new near infrared (NIR) tool for quantifying coffinite (USiO₄) in a moderately complex
415 uranium ore analogue. *J. Geochem. Explor.* 182, 80–93. doi:10.1016/j.gexplo.2017.09.003
- 416 Baron, F., Robin, V., Beaufort, D., Szenknect, S., Dacheux, N., Petit, S., 2014. Technical Note: Use of
417 near infrared spectroscopy for the identification of coffinite and uranothorite. *J. Infrared*
418 *Spectrosc.* 22, 149. doi:10.1255/jnirs.1110
- 419 Ben Simon, R., 2009. Experimental study and numerical modelling of geochemical reactions occurring
420 during uranium in situ recovery (ISR) mining. PhD thesis
- 421 Boulesteix, T., Cathelineau, M., Lach, P., Deloule, E., Brouand, M., Fiet, N., Toubon, H., 2015. Ilmenite
422 and their alteration products, sinkholes for uranium and radium in roll front deposits after
423 the example of South Tortkuduk (Kazakhstan). Presented at the 13th SGA biennial meeting,
424 Nancy.
- 425 Clark, R.N., Roush, T.L., 1984. Reflectance spectroscopy: Quantitative analysis techniques for remote
426 sensing applications. *J. Geophys. Res. Solid Earth* 89, 6329–6340.
- 427 Clavier, N., Szenknect, S., Costin, D., Mesbah, A., Poinssot, C., Dacheux, N., 2014. From thorite to
428 coffinite: A spectroscopic study of Th_{1-x}U_xSiO₄ solid solutions. *Spectrochim. Acta. A. Mol.*
429 *Biomol. Spectrosc.* 118, 302–307.
- 430 Dahlkamp, F.J., 2013, *Uranium ore deposits*. Springer Science & Business Media
- 431 Dahm, D.J., Dahm, K.D., 2001. The physics of near-infrared scattering. *-Infrared Technol. Agric. Food*
432 *Ind.* 2.
- 433 Delfosse-Ribay, E., Djeran-Maigre, I., Cabrillac, R., Gouvenot, D., 2004. Shear modulus and damping
434 ratio of grouted sand. *Soil Dyn. Earthq. Eng.* 24, 461–471. doi:10.1016/j.soildyn.2004.02.004

- 435 Dill, H.G., 2016. Kaolin: Soil, rock and ore: From the mineral to the magmatic, sedimentary and
436 metamorphic environments. *Earth-Sci. Rev.* 161, 16–129.
- 437 Ewing, R.C., 1994. The metamict state: 1993 — the centennial. *Nucl. Instrum. Methods Phys. Res.*
438 *Sect. B Beam Interact. Mater. At.* 91, 22–29. doi:10.1016/0168-583X(94)96186-7
- 439 French, M.W., Worden, R.H., 2013. Orientation of microcrystalline quartz in the Fontainebleau
440 Formation, Paris Basin and why it preserves porosity. *Sediment. Geol.* 284–285, 149–158.
441 doi:10.1016/j.sedgeo.2012.12.004
- 442 Geisler, T., Zhang, M., Salje, E.K.H., 2003. Recrystallization of almost fully amorphous zircon under
443 hydrothermal conditions: An infrared spectroscopic study. *J. Nucl. Mater.* 320, 280–291.
444 doi:10.1016/S0022-3115(03)00187-9
- 445 Gobrecht, A., Bendoula, R., Roger, J.-M., Bellon-Maurel, V., 2015. Combining linear polarization
446 spectroscopy and the Representative Layer Theory to measure the Beer–Lambert law
447 absorbance of highly scattering materials. *Anal. Chim. Acta* 853, 486–494.
448 doi:10.1016/j.aca.2014.10.014
- 449 Hauff, P., 2008. An overview of VIS-NIR-SWIR field spectroscopy as applied to precious metals
450 exploration. *Spectr. Int. Inc* 80001, 303–403.
- 451 Hebert, B., Beaufort, D., Roy, R., Pouradier, A., Jikibayev, R., 2015. New Methods to Quantify Clay
452 Minerals in the Uranium Deposits Hosted in Sands of the Chu Sarysu Basin (South
453 Kazakhstan) Based on Visible and Near-Infrared Field Spectrometry.
- 454 Herrmann, W., Blake, M., Doyle, M., Huston, D., Kamprad, J., Merry, N., Pontual, S., 2001. Short
455 wavelength infrared (SWIR) spectral analysis of hydrothermal alteration zones associated
456 with base metal sulfide deposits at Rosebery and Western Tharsis, Tasmania, and Highway-
457 Reward, Queensland. *Econ. Geol.* 96, 939–955.
- 458 Hunt, G.R., Ashley, R.P., 1979. Spectra of altered rocks in the visible and near infrared. *Econ. Geol.* 74,
459 1613–1629.
- 460 Hunt, G.R., Salisbury, J.W., 1970. Visible and near-infrared spectra of minerals and rocks : I silicate
461 minerals. *Mod. Geol.* 1, 283–300.
- 462 Klunder, G.L., Plaue, J.W., Spackman, P.E., Grant, P.M., Lindvall, R.E., Hutcheon, I.D., 2013.
463 Application of visible/near-infrared reflectance spectroscopy to uranium ore concentrates for
464 nuclear forensic analysis and attribution. *Appl. Spectrosc.* 67, 1049–1056.
- 465 Kruse, F.A., Boardman, J.W., Huntington, J.F., 2003. Comparison of airborne hyperspectral data and
466 eo-1 hyperion for mineral mapping. *IEEE Trans. Geosci. Remote Sens.* 41, 1388–1400.
467 doi:10.1109/TGRS.2003.812908
- 468 Lach, P., Cathelineau, M., Brouand, M., Fiet, N., 2015. In-situ isotopic and chemical study of pyrite
469 from Chu-Sarysu (Kazakhstan) roll-front uranium deposit. *Earth Planet. Sci. Lett.* 13, 207-210.
470 doi: 10.1016/j.proeps.2015.07.049
- 471 Mackey, D.J., Runciman, W.A., Vance, E.R., 1975. Crystal-field calculations for energy levels of U 4 + in
472 ZrSi O 4. *Phys. Rev. B* 11, 211–218. doi:10.1103/PhysRevB.11.211

- 473 Madejová, J., Pentrák, M., Pálková, H., Komadel, P., 2009. Near-infrared spectroscopy: A powerful
474 tool in studies of acid-treated clay minerals. *Vib. Spectrosc.* 49, 211–218.
475 doi:10.1016/j.vibspec.2008.08.001
- 476 Mathieu, R., Deschamps, Y., Selezneva, V., Pouradier, A., Brouand, M., Deloule, E., Boulesteix, T.,
477 2015. Key mineralogical characteristics of the new South Tortkuduk uranium roll-front
478 deposits, Kazakhstan. Presented at the 13th SGA biennial meeting, Nancy.
- 479 Mathieu, M., Roy, R., Launeau, P., 2017. Alteration mapping on drill cores using a HySpex SWIR-320m
480 hyperspectral camera: Application to the exploration of an unconformity-related uranium
481 deposit (Saskatchewan, Canada). *J Geochem Explor* 172:71–88
- 482 Mesbah, A., Szenknect, S., Clavier, N., Lozano-Rodriguez, J., Poinssot, C., Den Auwer, C., Ewing, R.C.,
483 Dacheux, N., 2015. Coffinite, $USiO_4$, Is Abundant in Nature: So Why Is It So Difficult To
484 Synthesize? *Inorg. Chem.* 54, 6687–6696. doi:10.1021/ic502808n
- 485 Munara, A., 2012. Formation des gisements d'uranium de type roll: approche minéralogique et
486 géochimique du gisement uranifère de Muyunkum (Bassin de Chu-Sarysu, Kazakhstan). PhD
487 327p.
- 488 Nasdala, L., Hanchar, J.M., Kronz, A., Whitehouse, M.J., 2005. Long-term stability of alpha particle
489 damage in natural zircon. *Chem. Geol.* 220, 83–103. doi:10.1016/j.chemgeo.2005.03.012
- 490 Pontual, S., Merry, N., Gamson, P., 1997. G-Mex Vol. 1, Spectral interpretation field manual. AusSpec
491 Int. Pty Ltd Kew Vic. 3101.
- 492 Post, J.L., Crawford, S.M., 2014. Uses of near-infrared spectra for the identification of clay minerals.
493 *Appl. Clay Sci.* 95, 383–387. doi:10.1016/j.clay.2014.02.010
- 494 Ramanaidou, E., Wells, M., Lau, I., Laukamp, C., 2015. Characterization of iron ore by visible and
495 infrared reflectance and, Raman spectroscopies, in: *Iron Ore: Mineralogy, Processing and
496 Environmental Sustainability*. Woodhead Publishing, pp. 191–228.
- 497 Robin, V., Hebert, B., Beaufort, D., Sardini, P., Tertre, E., Regnault, O., Descostes, M., 2015a.
498 Occurrence of authigenic beidellite in the Eocene transitional sandy sediments of the Chu-
499 Saryssu basin (South-Central Kazakhstan). *Sediment. Geol.* 321, 39–48.
500 doi:10.1016/j.sedgeo.2015.03.004
- 501 Robin, V., 2015b. Effet de la cristalochimie des minéraux argileux gonflants sur les propriétés
502 d'échange cationique et de dissolution. Implications dans un contexte de réhabilitation de
503 sites miniers acidifiés. PhD 190p.
- 504 Szenknect, S., Mesbah, A., Cordara, T., Clavier, N., Brau, H.-P., Le Goff, X., Poinssot, C., Ewing, R.C.,
505 Dacheux, N., 2016. First experimental determination of the solubility constant of coffinite.
506 *Geochim. Cosmochim. Acta* 181, 36–53. doi:10.1016/j.gca.2016.02.010
- 507 Xu, Q.-J., Ye, F.-W., Liu, S.-F., Zhang, Z.-X., Zhang, C., 2017. Hyperspectral Alteration Information from
508 Drill Cores and Deep Uranium Exploration in the Baiyanghe Uranium Deposit in the
509 Xuemisitan Area, Xinjiang, China. *Remote Sens.* 9, 451. doi:10.3390/rs9050451
- 510 Yazikov, V., 2002. Uranium raw material base of the Republic of Kazakhstan and prospects of using in
511 situ leach mining for its development. *Situ Leach Uranium Min.* T1-TC-975 IAEA Vienna 22–
512 31.

- 513 Zhang, F.X., Pointeau, V., Shuller, L.C., Reaman, D.M., Lang, M., Liu, Z., Hu, J., Panero, W.R., Becker,
514 U., Poinssot, C., Ewing, R.C., 2009. Structural transitions and electron transfer in coffinite,
515 USiO₄, at high pressure. *Am. Mineral.* 94, 916–920. doi:10.2138/am.2009.3111
- 516 Zhang, M., Salje, E.K., Ewing, R.C., 2003. Oxidation state of uranium in metamict and annealed zircon:
517 near-infrared spectroscopic quantitative analysis. *J. Phys. Condens. Matter* 15, 3445.